Electrochimica Acta 215 (2016) 114–125

Contents lists available at ScienceDirect

Electrochimica Acta

journal homepage: www.elsevier.com/locate/electacta

One-pot hydrothermal synthesis of porous nickel cobalt phosphides with high conductivity for advanced energy conversion and storage

Yu-Mei Hu[a], Mao-Cheng Liu[a,b,*], Yu-Xia Hu[c], Qing-Qing Yang[a], Ling-Bin Kong[b], Long Kang[b]

[a] State Key Laboratory of Advanced Processing and Recycling of Non-ferrous Metals, Lanzhou University of Technology, Lanzhou 730050, PR China
[b] School of Materials Science and Engineering, Lanzhou University of Technology, Lanzhou 730050, PR China
[c] School of Bailie Engineering &Technology, Lanzhou City University, Lanzhou 730070, PR China

ARTICLE INFO

Article history:
Received 4 June 2016
Received in revised form 14 August 2016
Accepted 16 August 2016
Available online 17 August 2016

Keywords:
nickel cobalt phosphides
particles
high electrical conductivity
asymmetric supercapacitor

ABSTRACT

High electrical conductivity is a vital factor to improve electrochemical performance of energy storage materials. In this work, bimetallic nickel cobalt phosphides with high electrical conductivity and different Ni/Co molar ratios are directly fabricated via a simple hydrothermal method. The samples show uniform teeny nanoparticles morphology and excellent electrochemical performance. The NiCoP sample exhibits the most prominent specific capacity (571 C g^{-1} at 1 A g^{-1}) and out-bound rate characteristic (72.8% capacity retention with a 20-fold increase in current densities), which can be attributed to the good crystallinity, larger specific surface area, and noteworthy intrinsic conductivity that convenient for fast electron transfer in active material and fleet reversible faradic reaction characteristics. Simultaneously, an optimal asymmetric supercapacitor based on NiCoP as positive and activated carbon as negative is assembled. It can achieve a high energy density of 32 Wh kg^{-1} (at a power density of 0.351 kW kg^{-1}) and prominent cycling stability with 91.8% initial capacity retention after 3000 cycles. It demonstrates that nickel cobalt phosphides are promising as energy storage materials. The study could also pave the way to explore a new class of bimetallic phosphides materials high electrical conductivity for electrochemical energy storage.

1. Introduction

With the rise of energy requirement on account of the rapid consumption of energy and demand exceeds supply of electronic devices, stimulating researchers to develop high performance energy storage devices [1–4]. Supercapacitors as a sort of energy storage system are the most promising reserve force compared to Li ion battery and NI-MH batteries on the basis of their high power density, fleet kinetics of charge propagation and longevity [5–9]. The properties of supercapacitors usually depend on electrode materials. Many researchers try hard to exploit new electrode material which could contribute the optimal electrochemical performance. In consideration of the customary non-ideal energy density of supercapacitors, an anticipant strategy is to seek an electrode material that satisfies high energy density without sacrificing the power density.

Ni-Co based battery-type materials have been widely studied recently in terms of providing abundant redox reaction lead to greater charge storage than double electrode layer [10–14]. For battery-type materials, cyclic voltammetry curves have distinct redox peaks and charge-discharge curves appear corresponding voltage platform. In spite of these battery-type materials are distinguishing to the true pseudocapacitance according to perfect rectangle (carbon material or MnO_2) [15], as positive electrode materials can combine the advantage of both supercapacitors (power density) and batteries (energy density) [16,17]. Therefore, this kind of materials is studied widely.

Compared with single metallic Ni or Co compounds, bimetallic Ni-Co compounds possess ameliorative properties. For instance, Wu *et al.* [18] synthesized $NiCo_2O_4$ possesses at least two magnitudes higher electrical conductivity than that of NiO and Co_3O_4. Chen et al. [19] synthesized the $Ni_xCo_{3-x}O_4$ samples exhibited higher capacitance than NiO and Co_3O_4 under the same conditions. Chen *et al.* [20] fabricated bimetallic nickel cobalt selenides show more outstanding capacity characteristic than NiSe and CoSe. Zhang *et al.* [21] studied hollow $Ni_xCo_{9-x}S_8$ urchins which displays higher electrical conductivities than cobalt sulfides (CoS_x),

* Corresponding author. Tel.: +86 0 931 2976579, fax: +86 0 931 2976578.
E-mail address: liumc@lut.cn (M.-C. Liu).

http://dx.doi.org/10.1016/j.electacta.2016.08.074
0013-4686/

nickel sulfides (NiS_x). The nickel-cobalt hydroxide has more excellent performance than monometallic hydroxides of Co $(OH)_2$ and $Ni(OH)_2$ [22–24]. Although these bimetallic Ni-Co compounds provide remarkable electrochemical performance, they suffered from poor electrical conductivity which is adverse for electrochemical energy storage. On one hand, low electrical conductivity could increase the IR potential drop of electrode in the large current charge-discharge possess, and seriously weaken the practical potential window of materials. On the other hand, low electrical conductivity prevents the rapid migration of electrons in great rate charge-discharge condition, and introducing severe electrochemical polarization, which could reduce the utilization efficiency of active materials. Thus, the electrical conductivity is a significant factor which determines property of super-capacitive materials. Enhancing electrical conductivity or exploiting new-style electrode materials with high electrical conductivity play an important role for improving the electrochemical property.

Ni-Co phosphides as a sort of submetallic alloy possess much higher intrinsic conductivity than oxide semiconductors, and have abundant natural resources as well as environmentally genial nature [25]. They were applied to some other fields in published papers. For example, Hemeda et al. [26] synthesized semi-crystalline NiCoP film and investigate its magnetic properties. Liu *et al.* [27] fabricated NiCoP hollow spheres applied to lithium ion batteries. Ni-Co phosphides as electrode material for super-capacitors have not been studies by researchers despite in fact that they have high electrical conductivity [28]. So Ni-Co phosphides just can be used as a new kind of electrode materials with high electrical conductivity.

Served as energy storage materials, monometallic nickel phosphides have been widely applied to supercapacitors [29,30], whereas cobalt phosphides are relatively few for supercapacitors [31]. Studies have shown that nickel phosphides have high specific capacity, while cobalt phosphides possess outstanding rate capability and cycle performance. The most important thing is that both of them have high intrinsic conductivity contribute to fleet charge storage. In order to combine high electrical conductivity, upper specific capacity, remarkable rate capability and cycle performance, it enlightens us designing and studying the electrochemical performance of Ni-Co phosphides. In this work, relied on one-step hydrothermal synthetic approach, a train of Ni-Co phosphides with high electrical conductivity and different Ni/Co molar ratios were synthesized and their electrochemical performance as positive materials for supercapacitors was investigated. It is found that Ni/Co molar ratios have a great influence on electrochemical properties of Ni-Co phosphides. The results showed that the Ni-Co phosphides, especially NiCoP possessed the highest specific capacity, high electrical conductivity, noteworthy rate capability and prominent cycle life, which indicated that NiCoP is an ideal electrochemical material and has great capacity for high-performance electrochemical energy storage systems. Besides, the AC//NiCoP asymmetrical supercapacitor attained both upper energy and power density, indicating superior performance of asymmetrical supercapacitor and active material in practical application.

2. Experimental section

Typical Ni-Co phosphides were synthesized via a hydrothermal process: a set number of $NiCl_2{\cdot}6H_2O$, $CoCl_2{\cdot}6H_2O$ and red phosphorus (200 °C 10 h hydrothermal pretreatment for the sake of thining grain size) were dissolved into 40 ml DI water along with continuous stirring. After ultra-sonication for 15 min, the hybrid suspension liquid decanted a 50 ml Teflon-lined stainless steel

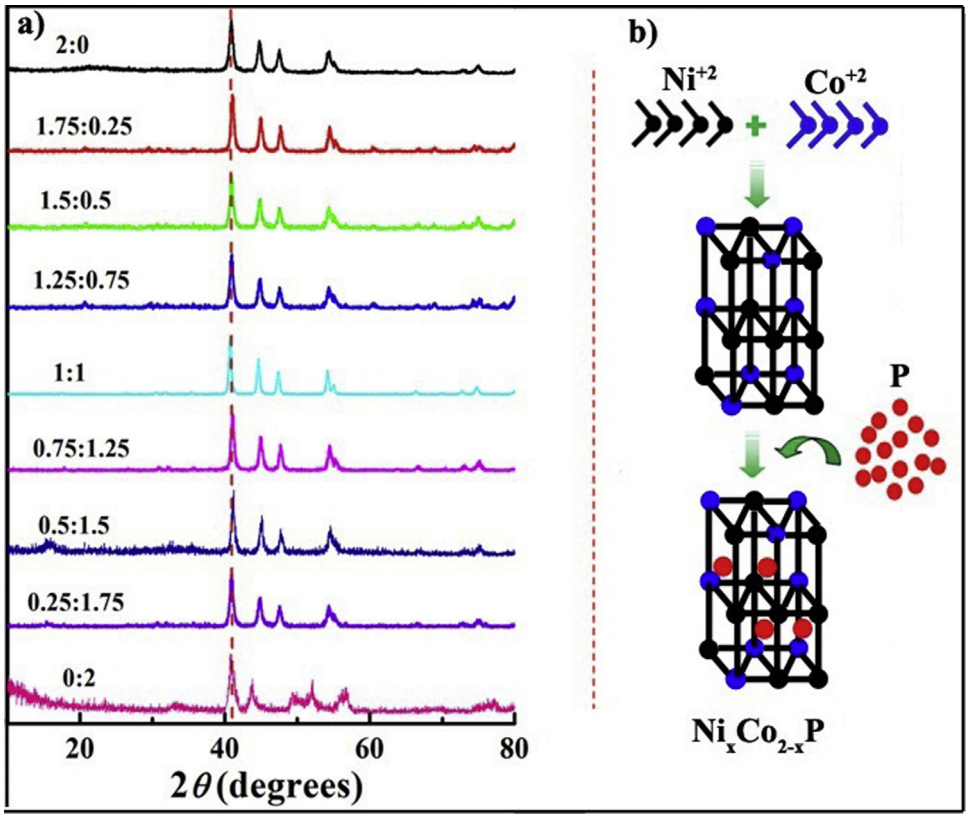

Fig. 1. (a) Typical XRD patterns of $Ni_xCo_{2-x}P$ with different Ni/Co molar ratios. (b) Schematic illustration of the formation mechanism of $Ni_xCo_{2-x}P$.

autoclave and kept at 200 °C for 10 h. The as-made samples were centrifuged and rinsed with DI water and Et-OH several times, and dried at 80 °C for 10 h. A train of Ni-Co phosphides with various theoretical Ni/Co molar ratios (marked $Ni_xCo_{2-x}P$) were synthesized by controlling the addition of raw materials. The working electrodes were prepared on the basis of our previous studies [32,33]. Relevant material characterizations, electrochemical evaluation and specific capacitance equation were shown in supplementary information.

3. Results and Discussion

3.1. Characterization of $Ni_xCo_{2-x}P$ particles

Fig. 1a presents the typical X-ray diffraction (XRD) patterns of $Ni_xCo_{2-x}P$ with different Ni/Co molar ratios. It is found that the Ni_2P (x = 2) and Co_2P (x = 0) possess legible diffraction peaks, which can be indexed as (111), (201), (210), (300) planes (PDF#03-0953) and (121), (211), (031), (320), (230) planes (PDF#32-0306), respectively (Fig. S1a,1b). However, it is interesting that all nickel cobalt phosphides with different Ni/Co molar ratios hold poignant diffraction peaks in keeping with Ni_2P nearly and the location of diffraction peaks is still uniform (marked red imaginary line). This phenomenon attests that all nickel cobalt phosphides have alike crystalline structure with Ni_2P. The diffraction peaks of NiCoP (Fig. S1c) can be indexed as (111), (201), (210), (300), (212) and (222) planes (PDF#71-2336), which is almost consistent with that of Ni_2P. It is because that the formation of $Ni_xCo_{2-x}P$ is derived from a part of Co^{2+} replace Ni^{2+} in Ni_2P. Hereby, schematic illustration of the formation of $Ni_xCo_{2-x}P$ particles is shown in Fig. 1b. It can be seen that metal atoms (Ni and Co) formed triangle prisms firstly and P atoms fill in the octahedral and tetrahedral interspaced of triangle prisms. This mechanism maintains the original structure framework of triangle prisms. Due to the formation of Ni_2P also derived from P atoms fill in the interspaced of triangle prisms. Thus the crystalline structure of $Ni_xCo_{2-x}P$ is similar to that of Ni_2P. Intuitively, this mechanism amount to a part of Co^{2+} replace Ni^{2+} in Ni_2P, which results all samples possess identical crystalline structure. The real Ni, Co contents in the final product $Ni_xCo_{2-x}P$ are tested by using ICP-OES and results are shown in Table S1 and Table S2. It can be seen that there is an obvious difference between the theoretical and real Ni/Co ratios in $Ni_xCo_{2-x}P$ samples. In the real Ni/Co ratios, Ni contents are much more than Co contents. This situation is because that the percent conversion of Co atoms is smaller than that of Ni atom in hydrothermal method. As described in Fig. 1b, a small quantity of Ni atoms is replaced by Co atoms in triangle prisms. Even so, the real Ni/Co ratios are also decrease gradually with increase of Co contents. The bimetallic nickel cobalt phosphides are synthesized certainly in spite of the Co contents is lesser.

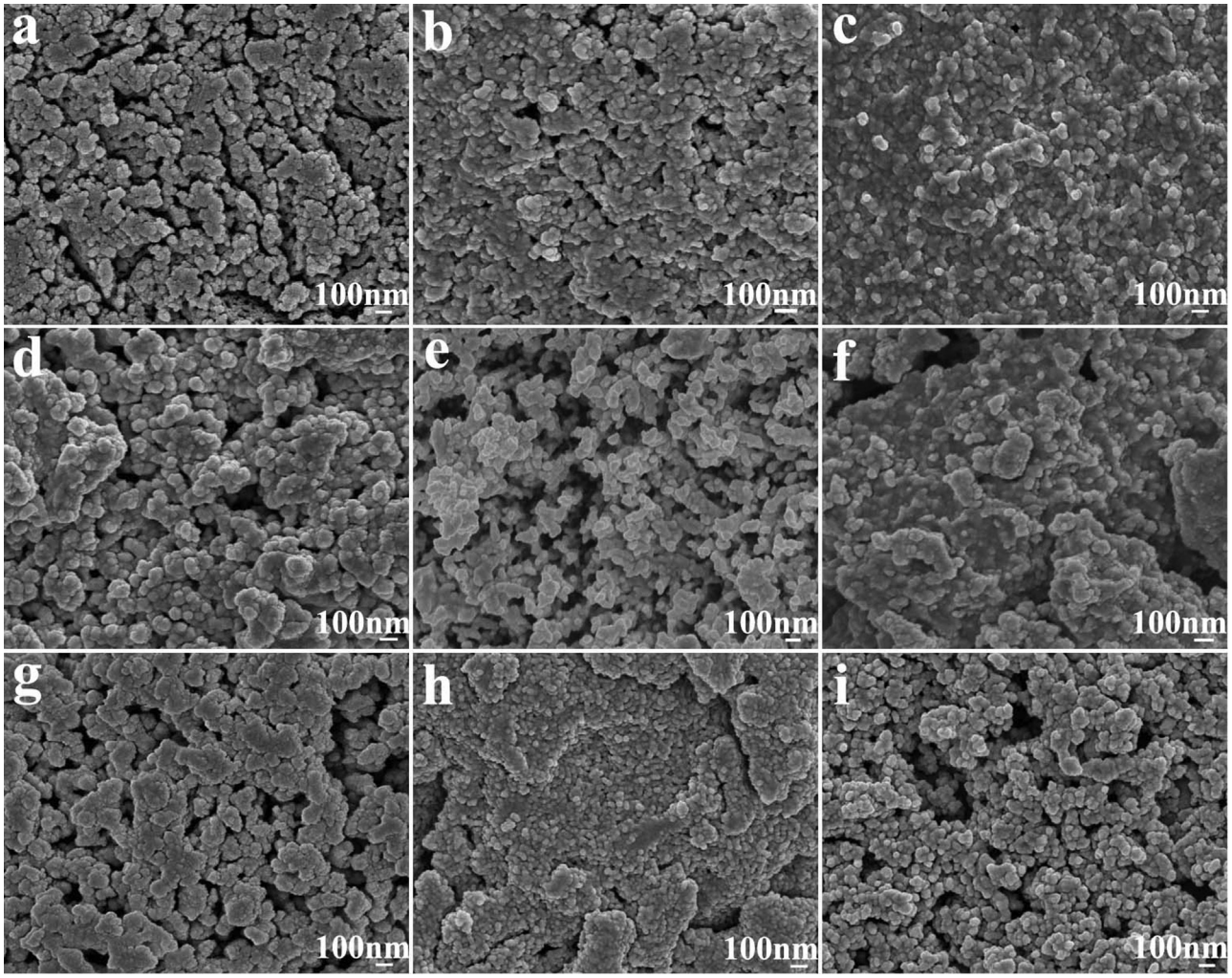

Fig. 2. Typical SEM images of $Ni_xCo_{2-x}P$ (x = 2, 1.75, 1.5 . . . 0) particles: (a) x = 2, (b) x = 1.75, (c) x = 1.5, (d) x = 1.25, (e) x = 1, (f) x = 0.75, (g) x = 0.5, (h) x = 0.25, and (i) x = 0.

The average crystallite size of samples from all lattice planes was computed employing the Debye-Scherer formula:

$$D = K\lambda/\beta\cos\theta \quad (1)$$

where D (nm) is the crystallite size, $K = 0.89$, λ is the wavelength of X-ray ($\lambda = 0.15406$ nm), β is the corrected full width at half maximum (FWHM) and θ is Bragg's angle. The average crystallite sizes of $Ni_xCo_{2-x}P$ (x = 2, 1.75, 1.5 . . . 0) are 16.7, 16.5, 21.8, 24.4, 21, 18, 20, 17.5 and 22 nm. The diminutive crystallite sizes of samples have great specific surface area and active sites, which is beneficial to sufficient contact between electrolyte and electroactive materials.

To observe the morphology and structure of the $Ni_xCo_{2-x}P$ (x = 2, 1.75, 1.5 . . . 0) particles with different Ni/Co molar ratios, the typical scanning electron microscopy (SEM) images were shown in Fig. 2. Results indicate that all samples appear uniform particles structure and the average sizes are pimping. Some samples emerge serious particle aggregation and even impenetrable grain wall (such as Fig. 2b, 2c, 2f, 2 h), which adverse to the diffusion of electrolyte ions. Nicely, the NiCoP (with Ni/Co molar ratio of 1:1) particles possess loosened multihole construction, which makes for shuttle back and forth of electrolyte and avoiding volume expansion in the process of faradaic reaction. The low-magnification SEM images of $Ni_xCo_{2-x}P$ (x = 2, 1.75, 1.5 . . . 0) particles are also shown in Fig. S2. All samples exhibit identical dense particles

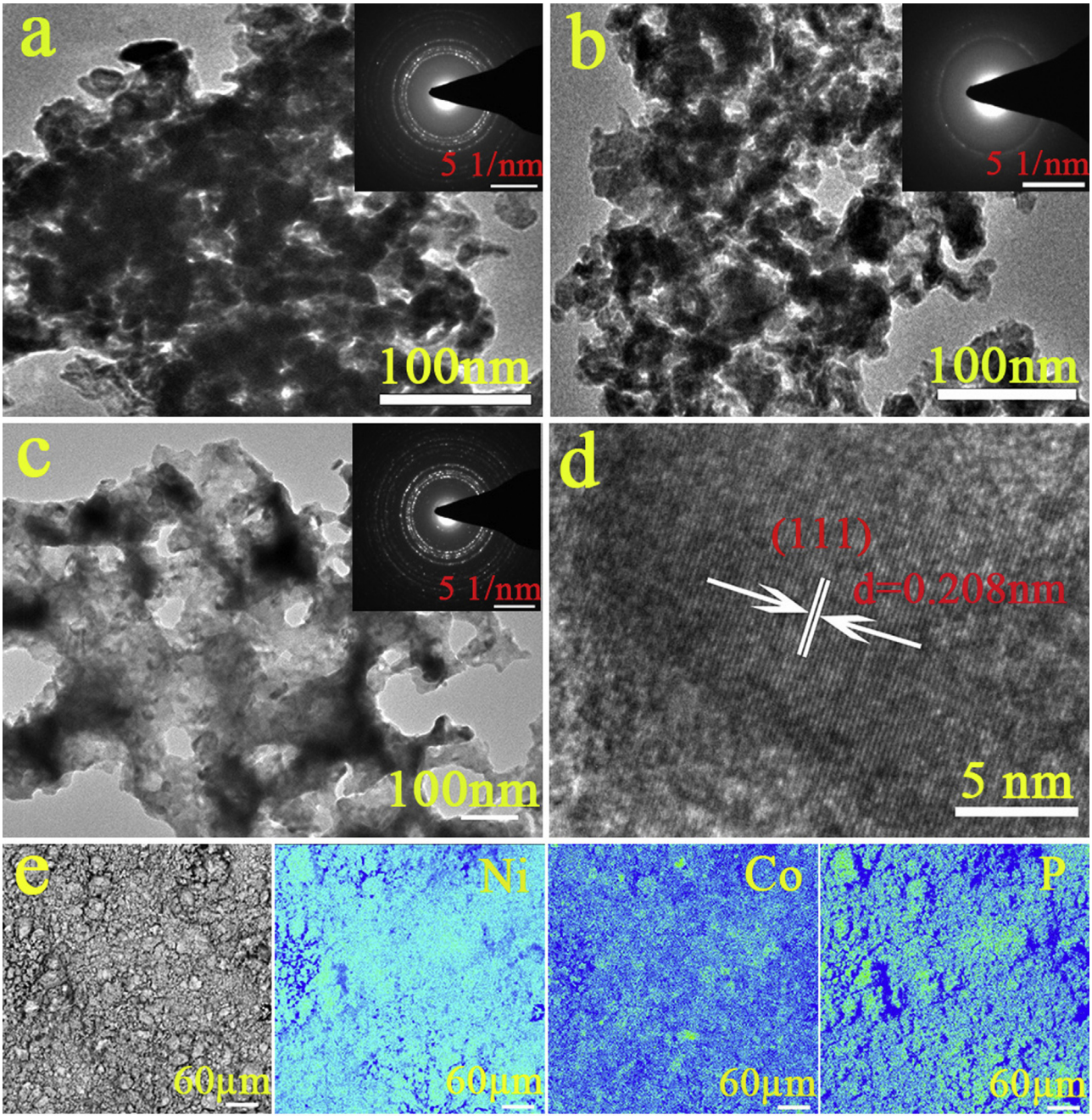

Fig. 3. (a,b) TEM images of the Ni_2P and Co_2P particles. (c) TEM (inset of SAED pattern) and (d) High resolution TEM image of the NiCoP particles with Ni/Co molar ratio of 1:1. (e) The electronic probe elemental mapping of NiCoP particles.

structure and the NiCoP sample (Fig. S2e) holds moss-like polyporous thicket composed of particles, which can provide great accessible area and active sites contributed to excellent electrochemical performance. The size distribution patterns of $Ni_xCo_{2-x}P$ samples by Zetasizer Nano 3600 are shown in Fig. S3 and the precise average sizes of all samples are shown in Table S3. Results reveal that the average sizes of all samples by Zetasizer Nano 3600 are larger than that of SEM results.

Transmission electron microscope (TEM) images of the Ni_2P and Co_2P particles are shown in Fig. 3a and 3b, both of them appear an unordered aggregated structure along with a mass of tunnels between particles. Abundant tunnels avail the rapid flow of electrolyte ions lead to facile charge storage. The selected area electron diffraction (SAED) pattern of Ni_2P (inset of Fig. 3a) and Co_2P (inset of Fig. 3a) appears some legible diffraction rings correspond to typical polycrystalline structure. The blurry diffraction rings of Co_2P demonstrate the inferior crystallinity. For NiCoP species (Fig. 3c), the relatively unfolded accumulation also exposes a mass of voids from the disordered distribution of particles. The SAED pattern of NiCoP (Fig. 3c, inset) is similar to the polycrystalline structure of Ni_2P (inset of Fig. 3a). This result future proves that nickel cobalt phosphides and Ni_2P have identical crystalline structure corresponding to the result of XRD. The high resolution TEM image of the NiCoP particles, as shown in Fig. 3b, arises unambiguous lattice fringes with estimated lattice plane space of 0.208 nm, which correspond to the (111) plane of NiCoP. For comparison, the high resolution TEM images of Ni_2P and Co_2P are shown Fig. S4a,4b. It can be seen that Ni_2P also has clear lattice fringes with lattice plane space of 0.2018 nm correspond to the (111) plane. However, there are discontinuous and vague fringes (marked red arrows) in Co_2P, which also attests a low crystallinity. It is corresponding to relatively broad diffraction peaks data in XRD pattern of Co_2P sample. Based on the above discussion, the NiCoP really possesses good crystallinity which could contribute to its high specific capacity and excellent rate capability in energy storage process. Elemental mappings from the electronic probe display a consistent distribution of Ni, Co, and P elements, indicating that the NiCoP is synthesized successfully (Fig. 3e).

The porosity and surface area of Ni_2P, Co_2P, NiCoP particles were characterized by the nitrogen adsorption-desorption isotherms as shown in Fig. S5. The pore size distribution curves demonstrate that the pores in Ni_2P and Co_2P possess some smaller mesopores from 2.5–4.3 nm mainly. The pores in NiCoP were abundant mesopores and a small quantity of macropores with a broad pore-size distribution. Macropores provide convenient passageway for the diffusion of ions while mesopores increase surface area of samples effectively. The surface area and pore volume of three samples were shown in Table 1. It can be seen that the NiCoP exhibits the largest surface area ($15.78\ m^2\ g^{-1}$) and medium pore volume ($0.0365\ cm^3\ g^{-1}$) among three samples. The electrode materials with a large specific surface area are found to deliver high specific capacitances [34]. The porous structure is beneficial to providing ample active sites and facilitates sufficient contact with electrolyte. Large size of holes avails the electrolyte ions quickly spread to the active material.

To future ascertain the chemical bonding states of every element in $Ni_xCo_{2-x}P$, NiCoP as a representative example is investigated by X-ray photoelectron spectroscopy (XPS) analysis (Fig. 4). Fig. 4a depicts the full spectrum of the NiCoP sample; the peaks can be identified as Ni, Co, P, O and C, which manifests that these elements exist in tested sample. The C element as master standard is added for peak position calibration and O element is derived from surface adsorption of sample when the sample is exposed to the air. Results revel the sample consists of Ni, Co, P elements on the surface, which is in line with our experiment. The Ni 2p spectra (Fig. 4b) shows two distinct peaks at binding energy of 856.6 eV and 874.5 eV assigned to the Ni $2p_{3/2}$ and Ni $2p_{1/2}$ peaks, which suggests the existence of Ni^{2+} [35–37]. For Co 2p spectra (Fig. 4c), the peaks centered at 797.98 eV for Co $2p_{1/2}$ and 781.87 eV for Co $2p_{3/2}$ are trait of Co^{2+} [38–40]. Future more, both of them possess two shake-up satellites (denoted as "Sat.") and appear ignorable peaks from $Ni^{3+}$and Co^{3+}. The trivalent parts may be derived from the inhomogeneity or partial oxidation of two ions on the surface scope. In the P 2p spectrum (Fig. 4d) of NiCoP particles, the peak at 129.6 eV may be assigned to $P^{\delta-}$ in the form of metal phosphide, and the broad peak at 133.3 eV is typical of phosphate species, likely due to superficial passivation of phosphide particles [41–43].

3.2. Electrochemical characterization of Ni-Co phosphides

In a general way, Co ions and Ni ions possess different electrochemical activity duo to the different variation of valence in redox reaction, which resulted in the discriminating contribution for specific capacity of compounds. Nickel cobalt phosphides with optimal electrochemical performance are exploited via harmonizing Ni/Co molar ratios. The specific capacity comparison at different current densities is shown in Fig. 5a. In most of Ni-Co compounds, Co ions usually put up the less electrochemical activity than Ni ions [44]. Therefore, the Co_2P shows the lowest specific capacity between all Ni-Co phosphides while the Ni_2P shows the highest specific capacity at $1\ A\ g^{-1}$. It is observed that the specific capacities increase gradually with the increase of Ni contents and attain optimal value in Ni/Co molar ratio of 1:1. However, the specific capacities decay when Ni contents further increase, which could be put down to the synergistic effect [45,46]. Corresponding specific capacity results at a current of $1\ A\ g^{-1}$ is shown in Table 2. The NiCoP achieves the highest specific capacity value between all Ni-Co phosphides which indicates a first-rank synergistic effect of Ni and Co ions. To be sure, Ni foam as current collector does not provide capacity nearly [47,48], so it is certain that almost all of the capacity stemmed from active materials. Even though Ni_2P has the highest specific capacity at $1\ A\ g^{-1}$, the rate capability is terrible. It also can be proved by the capacity retention at different current density (Fig. 5b). All samples keep 100% at normalized $1\ A\ g^{-1}$, and rate capability has obvious difference after current density of 20-fold increase. The corresponding capacity retentions are also shown in Table 2. Generally, the rate capability of nickel-based compounds is poor while cobalt-based compounds are excellent in many published studies [49]. This phenomenon also exists in this work; the Ni_2P holds the lowest capacity retention of 25.5% while the Co_2P has the highest capacity retention of 73.8%, which would declare that the rate capability of Ni-Co phosphides could be improved by the addition of Co ions. It

Table 1
Structural parameters of Ni_2P, Co_2P, and NiCoP particles.

Samples	BET specific surface area ($m^2\ g^{-1}$)	BJH specific pore volume ($cm^3\ g^{-1}$)	BJH mesopore size (nm)
Ni_2P	10.85	0.0215	3.4
Co_2P	8.43	0.1218	28.8
NiCoP	15.78	0.0365	3.3

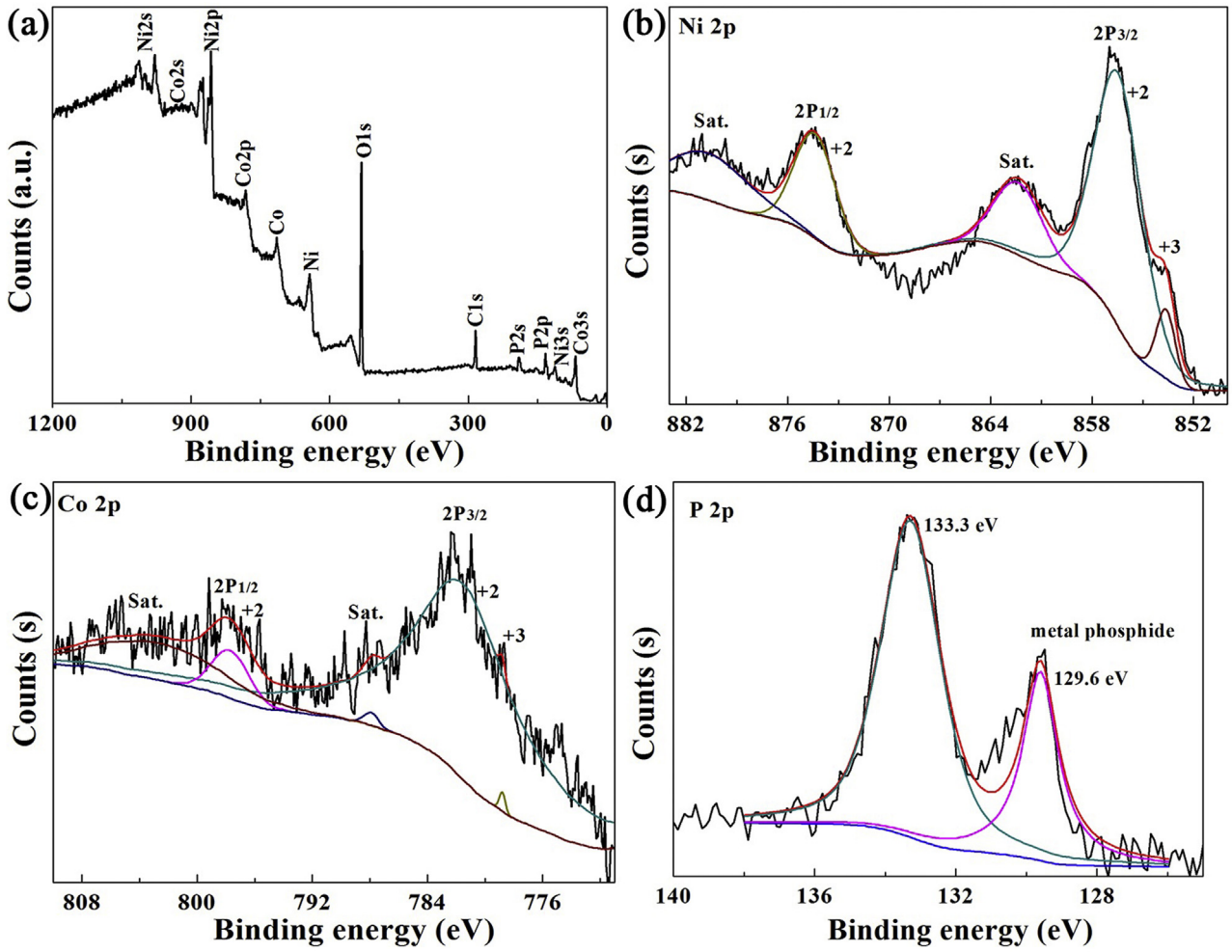

Fig. 4. XPS spectra of the NiCoP: (a) Survey spectrum, (b) Ni 2p, (c) Co 2p, and (d) P 2p.

is observed that the rate capability of all Ni-Co phosphides groups is more excellent than monometallic Ni_2P, and the NiCoP appears the best rate capability (72.8%) on account of the synergistic effect. The electrochemical properties of NiCoP as a representative further are examined. Fig. 5c gives the cyclic voltammetry (CV) curves comparison of Ni_2P, Co_2P, and NiCoP at a sweep rate of 5 mV s^{-1}. The Ni_2P puts up the largest current response with a pair of concentrated redox peaks, manifesting the faradaic characteristic of Ni_2P in electrochemical process. So it indicates that the Ni_2P belongs to battery-type materials. The charge storage mechanism in alkalic system could still be ascribed to the Ni^{2+}/Ni^{3+}, which can be described by the following equation:

$$Ni_2P + OH^- \leftrightarrow Ni_2POH + e^- \quad (2)$$

The Co_2P shows board redox peaks, which indicates the charge storage could occur in the whole potential window. The reactive mechanism could also be ascribed to the Co^{2+}/Co^{3+}, which can be described by the following equation:

$$Co_2P + OH^- \leftrightarrow Co_2POH + e^- \quad (3)$$

$$Co_2POH + OH^- \leftrightarrow Co_2PO + H_2O + e^- \quad (4)$$

In addition, the CV profiles of Ni_2P and Co_2P at various scan rates (Fig. S6) displays ordered variation at higher sweep rates. It can be seen the CV curve of NiCoP possesses a coordinating shade with subdued redox peaks compared to Ni_2P, which attests the combined action of Ni and Co ions. The CV area of an electrode material is proportional to its specific capacity. So this result corresponds to Fig. 5a. The Ni-Co phosphides also belongs to battery-type materials, it is similar to Ni-Co oxides [50–53], Ni-Co sulfides [54–56], and Ni-Co hydroxide [57,58]. Faradaic redox mechanism based on the following equation:

$$NiCoP + 2OH^- \leftrightarrow NiP_{1-x}OH + CoP_xOH + 2e^- \quad (5)$$

$$CoP_xOH + OH^- \leftrightarrow CoP_xO + H_2O + e^- \quad (6)$$

The cooperation of Ni and Co ions offers ample redox reactions lead to incremental specific capacity and rate capability. The CV curves of NiCoP can be observed that peaks positions come up excursion (Fig. 5d), which resulted from the internal resistance of electrode [59]. The relation curves between the scan rate square root and the cathodic (i_c) as well as anodic (i_a) peak currents are shown in Fig. 5e. It is found that the peak current depends linearly on the sweep rate square root, which indicates that the diffusion of the electrolyte is dominant in the redox process for NiCoP. Two curves are symmetrical based on i = 0 axis which indicates good reversibility of redox reaction. The specific capacities are calculated by charge-discharge curves (Fig. 5f) based on the formula $C_m = I\Delta t/m$ (in Supporting Information). In view of the battery-type materials, the unit of specific capacitance has been

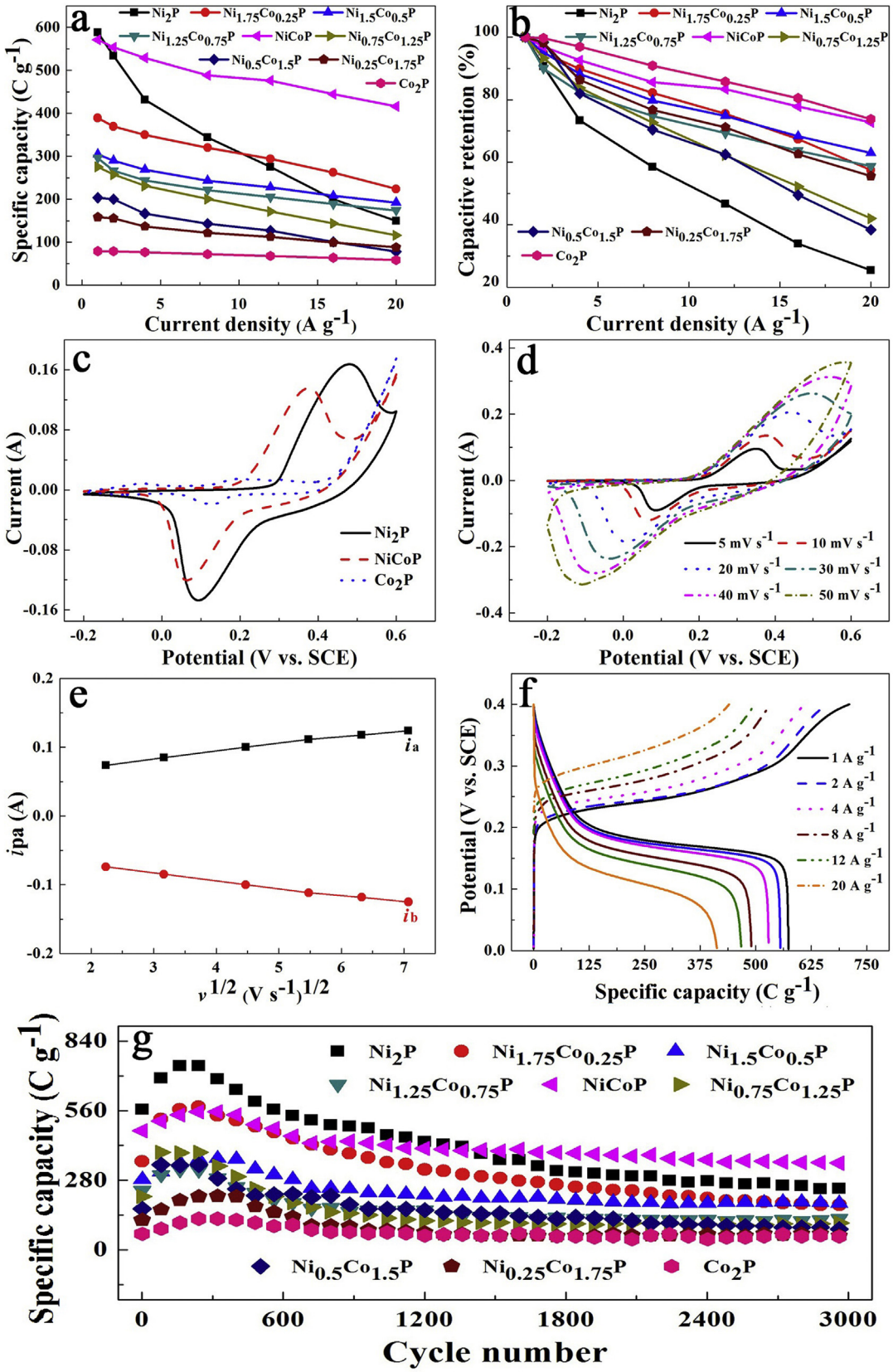

Fig. 5. (a) Specific capacity comparison at different current density and (b) Capacity retention of the $Ni_xCo_{2-x}P$ (x = 2, 1.75, 1.5 . . . 0). (c) The CV comparison of Ni_2P, Co_2P, and NiCoP at a scan rate of 5 mV s^{-1}. (d) CV curves of the NiCoP at different scan rates. (e) The relationship between the peak current and the sweep rates of the NiCoP electrode. (f) GCD curves of the NiCoP at different current densities. (g) Cycling stability of the $Ni_xCo_{2-x}P$ (x = 2, 1.75, 1.5 . . . 0).

Table 2
Electrochemical testing results of different samples.

Sample	Specific capacity (C g^{-1}, 1 A g^{-1})	Capacity retention from 1 to 20 A g^{-1} (%)	Capacity retention after 3000 cycles (%)
2:0	588	25.5	42
1.75:0.25.	389.1	57.6	51.4
1.5:0.5	304.5	63.1	66.2
1.25:0.75	296	58.8	53.1
1:1	571	72.8	71.8
0.75:1.25	275.6	42.1	50.1
0.5:1.5	203.4	38.4	52.5
0.25:1.75	158.4	55.6	51.7
0:2	79.2	73.8	76.7

defined as C g^{-1}, based on C $g^{-1} = \Delta V \cdot F\, g^{-1}$. The specific capacities of NiCoP are 571, 553.6, 528.8, 488.8, 476.4, and 416 C g^{-1} at current densities of 1, 2, 4, 8, 12, and 20 A g^{-1}, respectively. It is higher than Ni-Co oxides [60,61], Ni-Co sulfides [62,63], Ni-Co hydroxides [64] and other bimetallic compound [65–69]. In consideration of the long cycle life is an essential factor for energy storage systems; the cycling stability is tested at 2 A g^{-1}, as shown in Fig. 5 g. For the most of electrode materials, cycle life usually presents a trend of decline with the increase of cycle times. But in this work, all samples appear rising trend before 300 cycles, which can be put down to the activated process of electrode material. Then the cycling tends to be stable in subsequent cycles, relevant results are shown in Table 2. It is obvious that the Co_2P displays the best cycling stability of 76.7%, and the improved cycle performance of NiCoP (71.8%) is higher than other Ni-Co phosphides and Ni_2P. The results suggest that Co ions are beneficial for improving the cycle performance of Ni-Co phosphides. Except for the synergistic effect, optimal electrochemical performance of NiCoP also can be put down to the high intrinsic conductivity and abundant active sites originated from its loosely packed nanoparticles structure. In order to verify the structure stability of Ni-Co phosphides, the XRD and SEM tests of the optimal NiCoP, monometallic Ni_2P and Co_2P samples as representatives further are examined after 3000 charge-discharge cycles at 8 A g^{-1}, as shown in Fig. S7a-7f. It can be seen that the NiCoP, Ni_2P and Co_2P phases have on change before and after long cycles. The SEM results reveal they still hold nanoparticles morphology after 3000 cycles, which can further indicate the excellent cycling stability of Ni-Co phosphides.

The electrical conductivity as a decisive factor has a great improvement for electrochemical characteristics of electrode materials due to providing a high speed pathway for continuous electronic and ionic transportation. Fig. 6 shows the *I–V* curves and electrochemical impedance spectrum (EIS) analysis for the sake of inspect the influence of impedance on the electrochemical performance. The *I–V* curves of Co_2O_3, Ni_2P, graphite, Co_2P, and NiCoP present straight lines with different slope and the slope of lines is proportional to electrical conductivity of materials. Intuitively, the slope of Co_2P is the biggest, which indicates the highest electrical conductivity of it. The slope of Co_2O_3 is almost zero, proving the low electrical conductivity of metallic oxides. The NiCoP has moderate slope corresponding to its improved electrical conductivity; it is higher than Ni_2P and even graphite. The value of electrical conductivity can be estimated by the formula $G = 1/R$, $G = \kappa S/l$, where κ (S cm^{-1}) is electrical conductivity, R (Ω) is resistance; S (cm^2) and l (cm) are area and length of research electrode, respectively. Corresponding κ value of Co_2O_3, Ni_2P, graphite, NiCoP, and Co_2P are 0, 0.9, 0.83, 2.33, and 3.13 S cm^{-1}; results attests the excellent electrical conductivity of NiCoP. In order to further assess the electrical resistance of the Ni-Co phosphides, the Nyquist plots with high-resolution dates and equivalent circuit (inset) are shown in Fig. 6b. It can be observed that all curves are made up of unconspicuous semicircle in the high-frequency region and a straight line at the low-frequency region. The relation of impedance and frequency (Ω) can be

Table 3
Fitted parameters for EIS obtained by Zswinpwin software of different samples.

Sample	R_S (Ω)	R_{CT} (Ω)	W_0 (Ω)
Ni_2P	0.6736	0.2023	1.788
$Ni_{1.75}Co_{0.25}P$	0.6166	0.1097	2.356
$Ni_{1.5}Co_{0.5}P$.	0.5781	0.2206	0.772
$Ni_{1.25}Co_{0.75}P$	0.5465	0.0927	1.149
NiCoP	0.5054	0.0801	0.049
$Ni_{0.75}Co_{1.25}P$	0.4906	0.1332	1.988
$Ni_{0.5}Co_{1.5}P$	0.5244	0.2165	1.205
$Ni_{0.25}Co_{1.75}P$	0.5257	0.1533	1.792
Co_2P	0.5473	0.1394	2.685

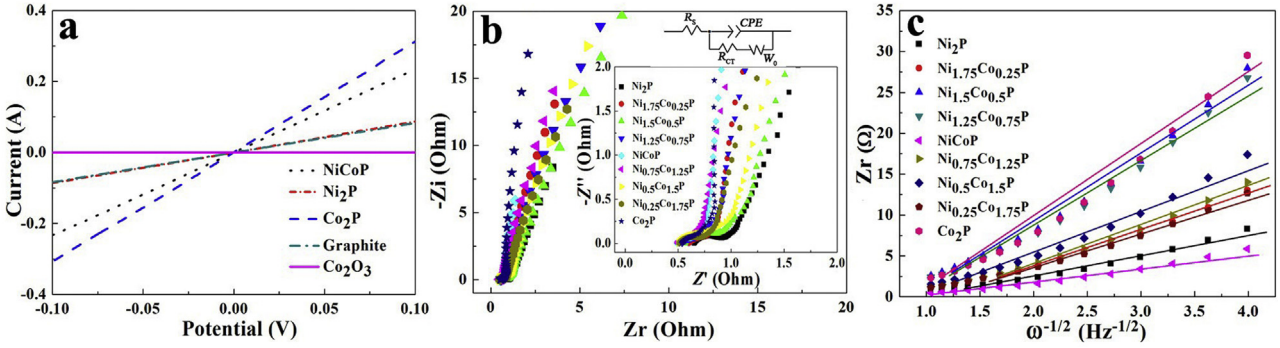

Fig. 6. (a) *I–V* curves of Co_2O_3, Ni_2P, graphite, Co_2P, and NiCoP. (b) Electrochemical impedance spectra for the $Ni_xCo_{2-x}P$ (x = 2, 1.75, 1.5 . . . 0). (c) Profiles of the real parts of impedance (*Zr*) *vs* $\Omega^{-1/2}$ from 0.1 to 0.01 Hz and corresponding linear fitting curves for $Ni_xCo_{2-x}P$ (x = 2, 1.75, 1.5 . . . 0).

evaluated according to formula below [70,71]:

$$Z = R_S + \frac{1}{\sqrt{-1}\omega + \frac{1}{R_{CT} + \frac{(1-\sqrt{-1})A}{\omega^{1/2}}}} \quad (7)$$

Suitable parameters for EIS acquired by Zswinpwin software of all species are shown in Table 3, which consist of the series resistance R_S, charge-transfer resistance R_{CT}, Warburg resistance W_o. Clearly, the R_{CT} value (0.0801 Ω) of NiCoP are the lower than monometallic Ni_2P, Co_2P and all Ni-Co phosphides, attesting that the cooperation of Ni and Co ions contribute to the diminution of the R_{CT}. The low R_{CT} of NiCoP also can be put down to the high electrical conductivity and outstanding rate capability, which could result in upper capacitive performance. In addition, the slope of all impedance plots at the low frequency region almost tends to vertical (the slope of curves exceed the standard Warburg slope of 1), which accords with low W_o. The NiCoP possesses the lowest W_o (0.049 Ω), indicating the toilless spread of electrolyte ions to the surface of the electrode and ideal capacitive behavior. The R_S can obtain from the point of intersection based on curve and real axis, which derived from electrolyte resistance and internal resistance of electrode. The R_S of NiCoP is the lowest (0.5054 Ω) between all Ni-Co phosphides except for $Ni_{0.75}Co_{1.25}P$ (0.4906 Ω). This situation is due to the NiCoP electrode is made up of numerous smaller particles, electron transfer between diminutive grains brings about the high contact resistance during the charge storage process [72]. Above results verify the high electrical conductivity of Ni-Co phosphides by coordinating Ni and Co components. The EIS tests of the long cycled NiCoP, monometallic Ni_2P and Co_2P electrodes as representatives further are examined in order to inspect the stability of samples (Fig. S7g–7i). The *R*s values of the NiCoP, Ni_2P and Co_2P only change 0.0035, 0.0415 and 0.0053 Ω after 3000 cycles, which can manifest a good conductivity of the electrolyte and the very low internal resistance of electrodes. The R_{CT} values change 0.0504, 0.0121 and0.0184 Ω after 3000 cycles, further investigation demonstrates that the Ni-Co phosphides exhibit excellent electrochemical cycling stability. Fig. 6c shows the linear profiles obtained from real part of impedance *Zr vs* $\Omega^{-1/2}$. Based on the formula below [73,74]:

$$Z\mathbf{r} = \sigma\omega^{-1/2} + k \quad (8)$$

Corresponding results of all samples are shown in Table 4. The Warburg factor σ could be obtained from the equation straight line. And future ions diffusion coefficients (Table 4) are obtained according to formula below:

$$D_0 = \frac{0.5R^2T^2}{n^4A^2F^4C^2\sigma^2} \quad (9)$$

Where *n* is the number of electron transfer during redox reaction, *A* is the surface area of electrode, *R* is the gas constant, *T* is the absolute temperature, *F* is the Faraday constant, *C* is the concentration of electrolyte. For certain, Ni_2P transfers one electron, Co_2P transfers two electrons and Ni-Co phosphides transfer three electrons. In view of *n* has a huge effect on the value diffusion coefficients, just compare diffusion coefficients of Ni-Co phosphides for fair. It can be seen that the diffusion coefficient of NiCoP (4.9×10^{-18} cm^2 s^{-1}) is minimum between Ni-Co phosphides, manifesting an heighten in the kinetics of ions diffusion in charge transfer reaction, which improve electrochemical property ultimately. Above all discussions confirm the high electrical conductivity of NiCoP, which has great significance for high-performance electrochemical energy storage devices.

Table 4
Corresponding results from (*Zr*) *vs* $\omega^{-1/2}$ profiles of different samples.

Sample	Linear equation	σ	Transfer electron number	D_0 (cm^2 s^{-1})
Ni_2P	y = 2.5x−2.5	2.5	1	1.6×10^{-16}
$Ni_{1.75}Co_{0.25}P$	y = 4.5x−5.1	4.5	3	6.2×10^{-19}
$Ni_{1.5}Co_{0.5}P$	y = 8.3x−7.2	8.3	3	1.8×10^{-19}
$Ni_{1.25}Co_{0.75}P$	y = 7.9x−7.1	7.9	3	2.0×10^{-19}
NiCoP	y = 1.6x−1.4	1.6	3	4.9×10^{-18}
$Ni_{0.75}Co_{1.25}P$	y = 4.9x−5.8	4.9	3	5.3×10^{-19}
$Ni_{0.5}Co_{1.5}P$	y = 5.1x−4.8	5.1	3	4.9×10^{-19}
$Ni_{0.25}Co_{1.75}P$	y = 3.8x−3.4	3.8	3	8.7×10^{-19}
Co_2P	y = 8.6x−6.8	8.6	2	8.6×10^{-19}

3.3. Electrochemical characterization of AC//NiCoP asymmetric supercapacitor

To inspect the worth of Ni-Co phosphides in practical applications, the asymmetric supercapacitor is fabricated based NiCoP as the positive electrode and AC as the negative electrode. Comparative CV curves of them at a scan rate of 10 mV s^{-1}, as shown in Fig. S8a, integrates a applicable voltage range of 1.6 V. When the voltage range is bigger than 1.6 V, the NiCoP electrode appears release oxygen and hydrogen. The specific capacity of AC at 1 A g^{-1} from charge-discharge curve (Fig. S8b) is 281 F g^{-1}. On the basis of specific capacity of NiCoP and AC, the mass ratio of positive and negative electrode is 0.62 based on the formula below:

$$\frac{m_+}{m_-} = \frac{C_- \times \Delta V_-}{C_+ \times \Delta V_+} \quad (10)$$

A simple model of asymmetric supercapacitor is shown in Fig. 7a, which could describe the construction of asymmetric supercapacitor vividly. Fig. 7b shows CV curves of asymmetric supercapacitor, the shape of curves is distinguished with perfect rectangle, it because that there is slight charge imbalance of two electrode. Charge-discharge curves (Fig. 7c) appear symmetrical charge-discharge profile with negligible voltage drop, indicating excellent capacitive performance of AC//NiCoP. The specific capacities of the AC//NiCoP capacitor can be evaluated from the charge-discharge curves based on the gross mass of active materials in two electrodes. Even so, a specific capacity reach to 164 C g^{-1} at 0.5 A g^{-1}, after 40-fold augment of current density, still maintains 93 C g^{-1} corresponding to 56.7% of the initial value (Fig. 7d). It manifests the out-bound rate capability of AC//NiCoP. The Ragone plot of the AC//NiCoP supercapacitor and AC//AC supercapacitor as contrast are shown in Fig. 7e. The energy and power density are assessed by the formula $E = 0.5C_mV/3.6$, $P = 3600E/\Delta t$. It is obvious that both energy and power density of AC//NiCoP are higher than AC//AC. The AC//NiCoP achieves a high energy density of 32 Wh kg^{-1} at a power density of 0.351 kW kg^{-1} and can still retain 18 Wh kg^{-1} when power density up to 5.586 kW kg^{-1}. It is higher than other Ni or Co-based hybrid supercapacitors, such as AC@Ni-P (29.4 Wh kg^{-1} at 0.4 kW kg^{-1}) [75], Ni-Co sulfide @AC (25 Wh kg^{-1} at 0.45 kW kg^{-1}) [76], core-shell $NiCo_2S_4$ @porous carbon (22.8 Wh kg^{-1} at 0.16 kW kg^{-1}) [77], porous $NiCoO_4$ @RGO (23.9 Wh kg^{-1} at 0.65 kW kg^{-1}) [78], graphene//Co_2P nanoflowers (24 Wh kg^{-1} at 0.3 kW kg^{-1}) [79], and $NiCo_2O_4$-rGO//AC (23.3 Wh kg^{-1} at 0.32 kW kg^{-1}) [31]. So the AC//NiCoP asymmetric supercapacitor is potential for high-performance electrochemical energy storage. Moreover, the cycle performance of AC//NiCoP at 2 A g^{-1} is investigated by the continuous charge-discharge tests, as shown in Fig. 7f, shows steady cycling charge-discharge ability of 91.8% after 3000 cycles. The GCD curves at different cycles (inset in Fig. 7f) exhibit almost overlapping shape originated from the unbroken structure of AC//NiCoP in repeating charge-discharge process. The AC//NiCoP displays high electrochemical reversibility and excellent cycling

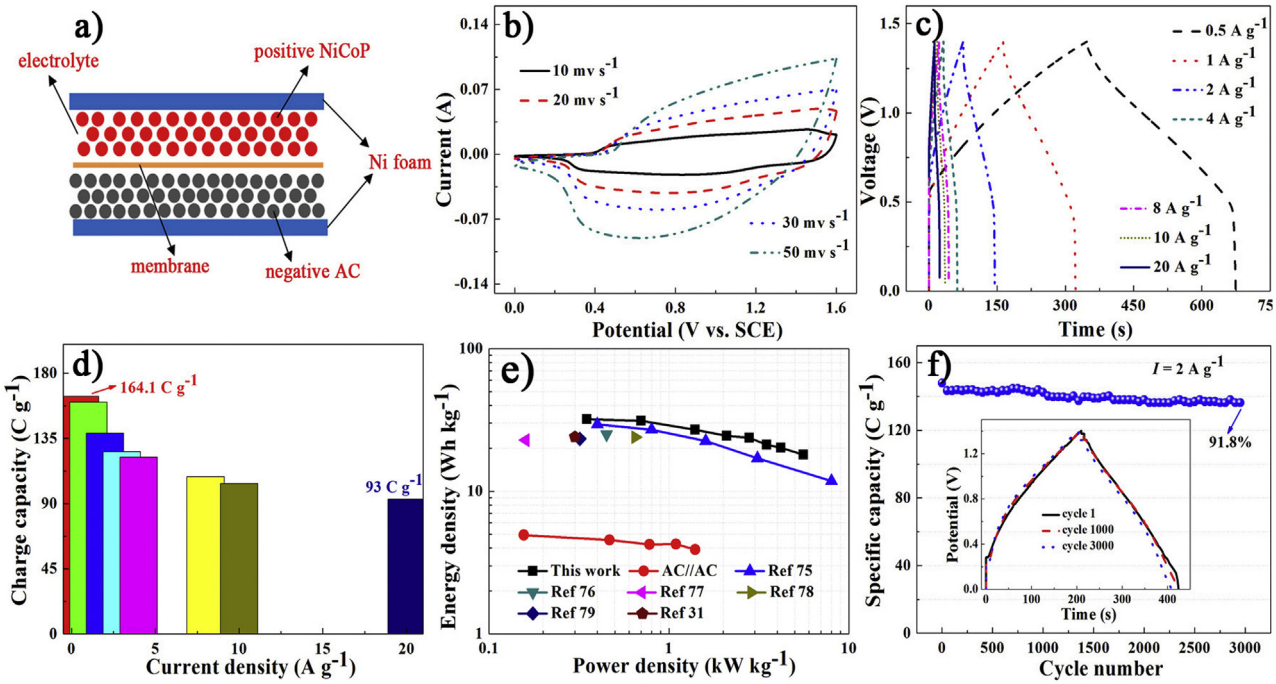

Fig. 7. (a) The simple model of asymmetric supercapacitor. (b) CV curves, (c) GCD curves, and (d) Specific capacity *vs* current density of AC//NiCoP. (e) Energy density *vs* power density. (f) Cycle performance of AC//NiCoP at 2 A g^{-1}.

stability. These results can adequately demonstrate the noteworthy property of asymmetric supercapacitor and active material in practical application.

4. Conclusion

In summary, the Ni-Co phosphides particles with high electrical conductivity and different Ni/Co molar ratios have been prepared via one-pot hydrothermal synthetic method. The electrochemical results revealed that the NiCoP has high electrical conductivity, which can speed up the electrolyte ion migration lead to outstanding electrochemical performance. The NiCoP achieves the highest specific capacity (571 C g^{-1} at 1 A g^{-1}) between all Ni-Co phosphides, exhibit out-bound rate capability and remarkable cycle life, which demonstrates an optimal synergistic effect for Ni and Co ions in their phosphides. The as AC//NiCoP asymmetrical supercapacitor shows a high specific energy of 32 Wh kg^{-1} at 0.351 kW kg^{-1}, manifesting a valuable practical application of this supercapacitor. This work provides a new path for other bimetallic phosphides in supercapacitor field.

Acknowledgment

This work was supported by the National Natural Science Foundation of China (no. 21403099), the Natural Science Foundation of Gansu Province (no. 145RJZA193), and the fund of the State Key Laboratory of Advanced Processing and Recycling of Non-ferrous Metals, Lanzhou University of Technology (no. SKLAB02014005).

Appendix A. Supplementary data

Supplementary data associated with this article can be found, in the online version, at http://dx.doi.org/10.1016/j.electacta.2016.08.074.

References

[1] T.W. Lin, C.S. Dai, T.T. Tasi, S.W. Chou, J.Y. Lin, H.H. Shen, High-performance asymmetric supercapacitor based on Co_9S_8/3D graphene composite and graphene hydrogel, Chem. Eng. J. 279 (2015) 241.
[2] Y.C. Zheng, Z.Q. Li, J. Xu, T.L. Wang, X. Liu, X.H. Duan, Y.J. Ma, Y. Zhou, C.H. Pei, Multi-channeled hierarchical porous carbon incorporated Co_3O_4 nanopillar arrays as 3D binder-free electrode for high performance supercapacitors, Nano Energy 20 (2016) 94.
[3] J. Cherusseri, K.K. Kar, Hierarchically mesoporous carbon nanopetal based electrodes for flexible supercapacitors with super-long cyclic stability, J. Mater. Chem. A 3 (2015) 21586.
[4] B.G.S. Raj, J.J. Wu, A.M. Asiri, S. Anandan, Hybrid SnO_2-Co_3O_4 nanocubes prepared via a $CoSn(OH)_6$ intermediate through a sonochemical route for energy storage applications, RSC Adv. 6 (2016) 33361.
[5] F.X. Ma, L. Yu, C.Y. Xu, X.W. (David) Lou, Self-supported formation of hierarchical $NiCo_2O_4$ tetragonal microtubes with enhanced electrochemical properties, Energy Environ. Sci. 9 (2016) 862.
[6] G.Q. Zhang, L. Yu, H.E. Hoster, X.W. (David) Lou, Synthesis of one-dimensional hierarchical NiO hollow nanostructures with enhanced supercapacitive performance, Nanoscale 5 (2013) 877.
[7] Z.Q. Niu, W.Y. Zhou, X.D. Chen, J. Chen, S.S. Xie, Highly compressible and all-solid-state supercapacitors based on nanostructured composite sponge, Adv. Mater. 27 (2015) 6002.
[8] H. Chen, L.F. Hu, M. Chen, Y. Yan, L.M. Wu, Nickel-cobalt layered double hydroxide nanosheets for high-performance supercapacitor electrode materials, Adv. Funct. Mater. 24 (2014) 934.
[9] K. Zhou, W.J. Zhou, L.J. Yang, J. Lu, S. Cheng, W.J. Mai, Z.H. Tang, L.G. Li, S.W. Chen, Ultrahigh-performance pseudocapacitor electrodes based on transition metal phosphide nanosheets array via phosphorization: a general and effective approach, Adv. Funct. Mater. 25 (2015) 7530.
[10] V.H. Nguyen, C. Lamiel, J.J. Shim, Hierarchical mesoporous graphene@Ni-Co-S arrays on nickel foam for high-performance supercapacitors, Electrochim. Acta 161 (2015) 351.
[11] Z.H. Yang, X. Zhu, K. Wang, G. Ma, H. Cheng, F.F. Xu, Preparation of. $NiCo_2S_4$ flaky arrays on Ni foam as binder-free supercapacitor electrode, Appl. Surf. Sci. 347 (2015) 690.
[12] L.Y. Lin, J.L. Liu, T.M. Liu, J.H. Hao, K.M. Ji, R. Sun, W. Zeng, Z.C. Wang, Growth-controlled $NiCo_2S_4$ nanosheet arrays with self-decorated nanoneedles for high-performance pseudocapacitors, J. Mater. Chem. A 3 (2015) 17652.
[13] C. Long, M.T. Zheng, Y. Xiao, B.F. Lei, H.W. Dong, H.R. Zhang, H. Hu, Y.L. Liu, Amorphous Ni-Co binary oxide with hierarchical porous structure for electrochemical capacitors, ACS Appl. Mater. Interfaces 7 (2015) 24419.
[14] G.Q. Zhang, H.B. Wu, H.E. Hoster, M.B. Chan-Park, X.W. (David) Lou, Single-crystalline $NiCo_2O_4$ nanoneedle arrays grown on conductive substrates as

binder-free electrodes for high-performance supercapacitors, Energy Environ. Sci. 5 (2012) 9453.
[15] P. Sivaraman, S.P. Mishra, D.D. Potphode, A.P. Thakur, K. Shashidhara, A.B. Samui, A.R. Bhattacharyy, A supercapacitor based on longitudinal unzipping of multi-walled carbon nanotubes for high temperature application, RSC Adv. 5 (2015) 83546.
[16] Q.W. Zhou, X.Y. Wang, Y. Liu, Y.M. He, Y.F. Gao, J.R. Liu, igh Rate capabilities of $NiCo_2O_4$-based hierarchical superstructures for rechargeable charge storage, J. Electrochem. Soc. 161 (2014) 1922.
[17] F. Zhang, T.F. Zhang, X. Yang, L. Zhang, K. Leng, Y. Huang, Y.S. Chen, A high-performance supercapacitor-battery hybrid energy storage device based on graphene-enhanced electrode materials with ultrahigh energy density, Energy Environ. Sci. 6 (2013) 1623.
[18] Z.B. Wu, Y.R. Zhu, X.B. Ji, $NiCo_2O_4$-based materials for electrochemical supercapacitors, J. Mater. Chem. A 2 (2014) 14759.
[19] S.R. Chen, M. Xue, Y.Q. Li, Y. Pan, L.K. Zhu, S.L. Qiu, Rational design and synthesis of $Ni_xCo_{3-x}O_4$ nanoparticles derived from multivariate MOF-74 for Supercapacitors, J. Mater. Chem. A 3 (2015) 20145.
[20] H.C. Chen, S. Chen, M.Q. Fan, C. Li, D. Chen, G.L. Tian, K.Y. Shu, Bimetallic nickel cobalt selenides: a new kind of electroactive material for high-power energy storage, J. Mater. Chem. A 3 (2015) 23653.
[21] Y.F. Zhang, C.C. Sun, H.Q. Su, W. Huang, X.C. Dong, N-doped carbon coated hollow $Ni_xCo_{9-x}S_8$ urchins for a high performance supercapacitor, Nanoscale 7 (2015) 3155.
[22] X.Q. Cai, X.P. Shen, L.B. Ma, Z.Y. Ji, C. Xua, A.H. Yuan, Solvothermal synthesis of Ni Co-layered double hydroxide nanosheets decorated on RGO sheets for high performance supercapacitor, Chem. Eng. J. 268 (2015) 251.
[23] X. Sun, G.K. Wang, H.T. Sun, F.Y. Lu, M.P. Yu, J. Lian, Morphology controlled high performance supercapacitor behaviour of the Ni-Co binary hydroxide system, J. Power Sources 238 (2013) 150.
[24] Y. Bai, W.Q. Wang, R.R. Wang, J. Sun, L. Gao, Controllable synthesis of 3D binary nickel-cobalt hydroxide/graphene/nickel foam as a binder-free electrode for high-performance supercapacitors, J. Mater. Chem. A 3 (2015) 12530.
[25] Y.M. Hu, M.C. Liu, Y.X. Hu, Q.Q. Yang, L.B. Kong, W. Han, J.J. Li, L. Kang, Design and synthesis of $Ni_2P/Co_3V_2O_8$ nanocomposite with enhanced electrochemical capacitive properties, Electrochim. Acta 190 (2016) 1041.
[26] O.M. Hemeda, A. Tawfik, A.H. El-Sayed, M.A. Hamad, Synthesis and Characterization of Semi-crystalline NiCoP Film, Nov. Magn. 28 (2015) 3629.
[27] S.L. Liu, C.L. Ma, L.B. Ma, H.Z. Zhang, Synthesis of NiCoP hollow spheres and its electrochemical property, Chem. Phys. Lett. 638 (2015) 52.
[28] D. Wang, L.B. Kong, M.C. Liu, Y.C. Luo, L. Kang, An approach to preparing Ni-P with different phases for use as supercapacitor electrode materials, Chem. Eur. J. 21 (2015) 1.
[29] W.M. Du, R.Q. Kang, P.B. Geng, X. Xiong, D. Li, Q.Q. Tian, H. Pang, New asymmetric and symmetric supercapacitor cells based on nickel phosphide nanoparticles, Mater. Chem. Phys. 165 (2015) 207.
[30] W.M. Du, S.H. Wei, K.K. Zhou, J.J. Guo, H. Pang, X.F. Qian, New asymmetric and symmetric supercapacitor cells based on nickel phosphide nanoparticles, Mater. Res. Bull. 61 (2015) 333.
[31] X.J. Chen, M. Cheng, D. Chen, R.M. Wang, Shape-controlled synthesis of Co_2P nanostructures and their application in supercapacitors, ACS Appl. Mater. Interfaces 8 (2016) 3892.
[32] J.J. Li, M.C. Liu, L.B. Kong, D. Wang, Y.M. Hu, W. Han, L. Kang, Advanced asymmetric supercapacitors based on $Ni_3(PO_4)_2$@GO and Fe_2O_3@GO electrodes with high specific capacitance and high energy density, RSC Adv. 5 (2015) 41721.
[33] X.J. Ma, L.B. Kong, W.B. Zhang, M.C. Liu, Y.C. Luo, L. Kang, Design and synthesis of 3D Co_3O_4@$MMoO_4$ (M = Ni Co) nanocomposites as high-performance supercapacitor electrodes, Electrochim. Acta 130 (2014) 660.
[34] Z. Yu, L. Tetard, L. Zhai, J. Thomas, Supercapacitor electrode materials: nanostructures from 0 to 3 dimensions, Energy Environ. Sci. 8 (2015) 702.
[35] W.M. Du, Z.Y. Wang, Z.Q. Zhu, S. Hu, X.Y. Zhu, Y.F. Shi, H. Pang, X.F. Qian, Facile synthesis and superior electrochemical performances of $CoNi_2S_4$/graphene nanocomposite suitable for supercapacitor electrodes, J. Mater. Chem. A 2 (2014) 9613.
[36] J. Kim, C.L. Jung, M. Kim, S. Kim, Y. Kang, H. Lee, J. Park, Y. Jun, D. Kim, Electrocatalytic activity of NiO on silicon nanowires with a carbon shell and its application in dye-sensitized solar cell counter electrodes, Nanoscale 8 (2016) 7761.
[37] S.S. Zhu, Y.M. Dai, W. Huang, C.X. Zhang, Y.Q. Zhao, L.H. Tan, Z.Z. Wang, In situ preparation of NiO nanoflakes on Ni foams for high performance Supercapacitors, Mater. Lett. 161 (2015) 731.
[38] R.J. Zou, K.B. Xu, T. Wang, G.J. He, Q. Liu, X.J. Liu, Z.Y. Zhang, J.Q. Hu, Chain-like $NiCo_2O_4$ nanowires with different exposed reactive planes for high-performance supercapacitors, J. Mater. Chem. A 1 (2013) 8560.
[39] J. Bai, X.G. Li, G.Z. Liu, Y.T. Qian, S.L. Xiong, Unusual Formation of $ZnCo_2O_4$ 3D Hierarchical twin microspheres as a high-rate and ultralong-life lithium-ion battery anode material, Adv. Funct. Mater. 24 (2014) 3012.
[40] M. Kim, I. Oh, H. Ju, J. Kim, Introduction of Co_3O_4 into activated honeycomb-like carbon for the fabrication of high performance electrode materials for supercapacitors, Phys. Chem. Chem. Phys. 18 (2016) 9124.
[41] Y. Zhou, R.G. Ma, S.L. Candelaria, J.C. Wang, Q. Liu, E. Uchaker, P.X. Li, Y.F. Chen, G.Z. Cao, Phosphorus/sulfur Co-doped porous carbon with enhanced specific capacitance for supercapacitor and improved catalytic activity for oxygen reduction reaction, J. Power Sources 314 (2016) 39.
[42] X. Yu, Y.B. Kang, H.S. Park, Sulfur and phosphorus co-doping of hierarchically porous graphene aerogels for enhancing supercapacitor performance, Carbon 101 (2016) 49.
[43] Z. Liu, J.H. Mi, Y. Yang, X.L. Tan, C. Lv, Easy synthesis of phosphorus-incorporated three-dimensionally ordered macroporous carbons with hierarchical pores and their use as electrodes for supercapacitors, Electrochim. Acta 115 (2014) 206.
[44] J. Xu, Y.Z. Dong, J.Y. Cao, B. Guo, W.C. Wang, Z.D. Chen, Microwave-incorporated hydrothermal synthesis of urchin-like $Ni(OH)_2$-$Co(OH)_2$ hollow microspheres and their supercapacitor applications, Electrochim. Acta 114 (2013) 76.
[45] X. Gong, J.P. Cheng, F. Liu, L. Zhang, X. Zhang, Nickel-Cobalt hydroxide microspheres electrodepositioned on nickel cobaltite nanowires grown on Ni foam for high-performance pseudocapacitors, J. Power Sources 267 (2014) 610.
[46] G. Chen, S.S. Liaw, B.S. Li, Y. Xu, M. Dunwell, S.G. Deng, H.Y. Fan, H.M. Luo, Microwave-assisted synthesis of hybrid $Co_xNi_{1-x}(OH)_2$nanosheets: Tuning the composition for high performance supercapacitor, J. Power Sources 251 (2014) 338.
[47] P.P. Xu, K. Ye, D.X. Cao, J.C. Huang, T. Liu, K. Cheng, J.L. Yin, G.L. Wang, Facile synthesis of cobalt manganese oxides nanowires on nickel foam with superior electrochemical performance, J. Power Sources 268 (2014) 204.
[48] X.X. Liu, C.D. Shi, C.W. Zhai, M.L. Cheng, Q. Liu, G.X. Wang, Cobalt-based layered metal-organic framework as an ultrahigh capacity supercapacitor electrode material, ACS Appl. Mater. Interfaces 8 (2016) 4585.
[49] M.C. Liu, L.B. Kong, L. Kang, X.H. Li, F.C. Walsh, M. Xing, C. Lu, X.J. Ma, Y.C. Luo, Synthesis and characterization of $M_3V_2O_8$ (M = Ni or Co) based nanostructures: a new family of high performance pseudocapacitive materials, J. Mater. Chem. A 2 (2014) 4919.
[50] E. Umeshbabu, G. Rajeshkhanna, G.R. Rao, Synthesis and electrochemical energy storage application, Int. J. Hydrogen Energy 39 (2014) 15627.
[51] E. Umeshbabua, G. Rajeshkhanna, P. Justin, G.R. Rao, Magnetic, optical and electrocatalytic properties of urchin and sheaf-like $NiCo_2O_4$ nanostructures, Mater. Chem. Phys. 165 (2015) 235.
[52] J.F. Shen, X.F. Li, N. Li, M.X. Ye, Facile synthesis of $NiCo_2O_4$-reduced graphene oxide nanocomposites with improved electrochemical properties, Electrochim. Acta 141 (2014) 126.
[53] H.B. Wu, H. Pang, X.W. (David) Lou, Facile synthesis of mesoporous $Ni_{0.3}Co_{2.7}O_4$ hierarchical structures for high-performance supercapacitors, Energy Environ. Sci. 6 (2013) 3619.
[54] R. Ding, M.Y. Zhang, Y.H. Yao, H. Gao, Crystalline $NiCo_2S_4$ nanotube array coated with amorphous $NiCo_xS_y$ for supercapacitor electrodes, J. Colloid Interface Sci. 467 (2016) 140.
[55] Z.F. Zeng, D.Z. Wang, J.L. Zhu, F.Q. Xiao, Y.D. Li, X.H. Zhu, $NiCo_2S_4$ nanoparticles// activated balsam pear pulp for asymmetric hybrid capacitors, Crystengcomm 18 (2016) 2363.
[56] L.W. Mi, W.T. Wei, S.B. Huang, S.Z. Cui, W.X. Zhang, H.W. Hou, W.H. Chen, A nest-like Ni@$Ni_{1.4}Co_{1.6}S_2$ electrode for flexible high-performance rolling supercapacitor device design, J. Mater. Chem. A 3 (2015) 20973.
[57] Z.Q. Liu, G.F. Chen, P.L. Zhou, N. Li, Y.Z. Su, Building layered $NixCo_{2x}(OH)_{6x}$ nanosheets decorated three-dimensional Ni frameworks for electrochemical applications, J. Power Sources 317 (2016) 1.
[58] C.Q. Shang, S.M. Dong, S. Wang, D.D. Xiao, P.X. Han, X.G. Wang, L. Gu, G.L. Cui, Coaxial $Ni_xCo_{2x}(OH)_{6x}$/TiN Nanotube Arrays as Supercapacitor Electrodes, ACS Nano 7 (2013) 5430.
[59] R. Bendi, V. Kumar, V. Bhavanasi, K. Parida, P.S. Lee, Metal organic framework-derived metal phosphates as electrode materials for supercapacitors, Adv. Energy Mater. 6 (2016) 1501833.
[60] S. Khalid, C.B. Cao, L. Wang, Y.Q. Zhu, Microwave Assisted Synthesis of Porous $NiCo_2O_4$ Microspheres: Application as High Performance Asymmetric and Symmetric Supercapacitors with Large Areal Capacitance, Sci. Rep. 6 (2016) 22699.
[61] D.S. Sun, Y.H. Li, Z.Y. Wang, X.P. Cheng, S. Jaffer, Y.F. Zhang, Understanding the mechanism of hydrogenated $NiCo_2O_4$ nanograss supported on Ni foam for enhanced-performance supercapacitors, J. Mater. Chem. A 4 (2016) 5198.
[62] H.C. Chen, J.J. Jiang, Y.D. Zhao, L. Zhang, D.Q. Guo, D.D. Xia, One-pot synthesis of porous nickel cobalt sulphides: tuning the composition for superior pseudocapacitance, J. Mater. Chem. A 3 (2015) 428.
[63] V.H. Nguyen, C. Lamiel, J.J. Shim, Hierarchical mesoporous graphene@Ni-Co-S arrays on nickel foam for high-performance supercapacitors, Electrochim. Acta 161 (2015) 351.
[64] X.R. Su, Y.Y. Xu, J.L. Liu, R.M. Wang, Controlled synthesis of $Ni_{0.25}Co_{0.75}$ $(OH)_2$ nanoplates and their electrochemical properties, Crystengcomm 17 (2015) 4859.
[65] J.F. Shen, J.H. Tang, P. Dong, Z.Q. Zhang, J. Ji, R. Baines, M.X. Ye, Construction of three-dimensional $CuCo_2S_4$/CNT/graphene nanocomposite for high performance supercapacitors, RSC Adv. 6 (2016) 13456.
[66] X.D. Yan, L.H. Tian, J. Murowchick, X.B. Chen, Partially amorphized $MnMoO_4$ for highly efficient energy storage and the hydrogen evolution reaction, J. Mater. Chem. A 4 (2016) 3683.
[67] Y. Ma, Y.L. Jia, L.N. Wang, M. Yang, Y.P. Bi, Y.X. Qi, Facile growth of Bi_2MoO_6 nanosheet arrays on Ni foam as an electrode for electrochemical applications, RSC Adv. 6 (2016) 12093.
[68] Y.H. Dai, L.B. Kong, Kun Yan, M. Shi, T. Zhang, Y.C. Luo, L. Kang, Simple synthesis of a $CoMoS_4$ based nanostructure and its application for high-performance supercapacitors, RSC Adv. 6 (2016) 7633.

[69] C.S. Wang, Y. Xi, C.G. Hu, S.G. Dai, M.J. Wang, L. Cheng, W.N. Xu, G. Wang, W.L. Li, β-$NiMoO_4$ nanowire arrays grown on carbon cloth for 3D solid asymmetry supercapacitors, RSC Adv. 5 (2015) 107098.
[70] X.J. Ma, W.B. Zhang, L.B. Kong, Y.C. Luo, L. Kang, Pseudocapacitance of ammonium metavanadate pyrolysis products, Electrochim Acta 192 (2016) 30.
[71] X. Li, J. Rong, B. Wei, Electrochemical behavior of single-walled carbon nanotube supercapacitors under compressive stress, ACS Nano 4 (2010) 6039.
[72] C.R. Zheng, C.B. Cao, Z. Alia, J.H. Hou, Enhanced electrochemical performance of ball milled CoO for supercapacitor applications, J. Mater. Chem. A 2 (2014) 16467.
[73] D. Luo, G.S. Li, X.F. Guan, C. Yu, J. Zheng, X.H. Zhang, L.P. Li, Novel synthesis of $Li_{1.2}Mn_{0.4}Co_{0.4}O_2$ with an excellent electrochemical performance from −10.4 to 45.4 °C, J. Mater. Chem. A 1 (2013) 1220.
[74] X.H. Zhang, D. Luo, G.S. Li, J. Zheng, C. Yu, X.F. Guan, C.C. Fu, X.D. Huang, L.P. Li, Self-adjusted oxygen-partial-pressure approach to the improved electrochemical performance of electrode $Li[Li_{0.14}Mn_{0.47}Ni_{0.25}Co_{0.14}]O_2$ for lithium-ion batteries, J. Mater. Chem. A 1 (2013) 9721.
[75] D. Wang, L.B. Kong, M.C. Liu, W.B. Zhang, Y.C. Luo, L. Kang, Amorphous Ni-P materials for high performance pseudocapacitors, J. Power Sources 274 (2015) 1107.
[76] Y.H. Li, L.J. Cao, L. Qiao, M. Zhou, Y. Yang, P. Xiao, Y.H. Zhang, Ni-Co sulfide nanowires on nickel foam with ultrahigh capacitance for asymmetric Supercapacitors, J. Mater. Chem. A 2 (2014) 6540.
[77] W. Kong, C.C. Lu, W. Zhang, J. Pu, Z.H. Wang, Homogeneous core-shell $NiCo_2S_4$ nanostructure supported on nickel foam for supercapacitors, J. Mater. Chem. A 3 (2015) 12452.
[78] H.C. Chen, J.J. Jiang, L. Zhang, T. Qi, D.D. Xia, H.Z. Wan, Facilely synthesized porous $NiCo_2O_4$ flowerlike nanostructure for high-rate supercapacitors, J. Power Sources 248 (2014) 28.
[79] X. Wang, W.S. Liu, X.H. Lu, P.S. Lee, Dodecyl sulfate induced fast faradic process in nickel cobalt oxide-reduced graphite oxide composite material and its application for asymmetric supercapacitor device, J. Mater. Chem. 22 (2012) 23114.